

Article

# Effect of the Thermodynamic Behavior of Selective Laser Melting on the Formation of In situ Oxide Dispersion-Strengthened Aluminum-Based Composites

Lianfeng Wang<sup>1,4,5</sup>, Jiubin Jue<sup>2,3</sup>, Mujian Xia<sup>2,3</sup>, Lijie Guo<sup>1,5</sup>, Biao Yan<sup>4</sup> and Dongdong Gu<sup>2,3,\*</sup>

<sup>1</sup> Shanghai Aerospace Equipments Manufacturer, Shanghai 200245, China; wlf149@163.com (L.W.); guolijie149@163.com (L.G.)

<sup>2</sup> College of Materials Science and Technology, Nanjing University of Aeronautics and Astronautics, Yuda Street 29, Nanjing 210016, China; jiubinjue@hotmail.com (J.J.); xmjnuaa@nuaa.edu.cn (M.X.)

<sup>3</sup> Institute of Additive Manufacturing (3D Printing), Nanjing University of Aeronautics and Astronautics, Yuda Street 29, Nanjing 210016, China

<sup>4</sup> Material Science and Engineering Department, Tongji University, Shanghai 200092, China; 84016@tongji.edu.cn

<sup>5</sup> Shanghai Research Center of Complex Metal Parts by Additive Manufacturing, Shanghai 200245, China

\* Correspondence: dongdonggu@nuaa.edu.cn; Tel.: +86-25-5211-2626

Academic Editor: Manoj Gupta

Received: 18 July 2016; Accepted: 9 November 2016; Published: 19 November 2016

**Abstract:** This paper presents a comprehensive investigation of the phase and microstructure, the thermodynamic behavior within the molten pool, and the growth mechanism of in situ oxide dispersion-strengthened (ODS) aluminum-based composites processed by a selective laser melting (SLM) additive manufacturing/3D printing process. The phase and microstructure were characterized by X-ray diffraction (XRD) and a scanning electronic microscope (SEM) equipped with EDX, respectively. The thermodynamic behavior within the molten pool was investigated for a comprehensive understanding on the growth mechanism of the SLM-processed composite using a finite volume method (FVM). The results revealed that the in situ  $\text{Al}_2\text{Si}_4\text{O}_{10}$  ODS Al-based composites were successfully fabricated by SLM. Combined with the XRD spectrum and EDX analysis, the new silica-rich  $\text{Al}_2\text{Si}_4\text{O}_{10}$  reinforcing phase was identified, which was dispersed around the grain boundaries of the aluminum matrix under a reasonable laser power of 200 W. Combined with the activity of Marangoni convection and repulsion forces, the characteristic microstructure of SLM-processed  $\text{Al}_2\text{Si}_4\text{O}_{10}$  ODS Al-based composites tended to transfer from the irregular network structure to the nearly sphere-like network structure in regular form by increasing the laser power. The formation mechanism of the microstructure of SLM-processed  $\text{Al}_2\text{Si}_4\text{O}_{10}$  ODS Al-based composites is thoroughly discussed herein.

**Keywords:** selective laser melting; aluminum matrix composites; microstructure; thermodynamic behavior; formation mechanism

## 1. Introduction

Aluminum matrix composites (AMCs) have been widely used in many applications, especially in the aerospace, defense, and automobile industries, due to its unique combination of light weight, high specific strength, and excellent wear performance [1]. Nevertheless, the limited wear resistance and other mechanical properties become a serious barrier for the application where abrasive and erosion phenomena exist. Thus, a considerable number of previous efforts have been attempted

to prepare ceramic particle reinforced aluminum matrix composites, coatings, or both to improve the corresponding properties of aluminum [2]. Normally, in order to enhance the performance of aluminum, the ceramic particles are employed as reinforcements to be directly added to the molten aluminum. For instance, the additive of  $\text{Al}_2\text{O}_3$  and  $\text{B}_4\text{C}$  ceramic particles were added to the aluminum composites to strengthen the mechanical properties [3]. However, owing to the considerably poor wettability between ceramics particle and aluminum, a poor interfacial bonding between the reinforcements and the matrix is generated, which considerably influences the mechanical performances of the AMCs. In the literature, the in situ synthesis of the reinforcements of the particle-reinforced metal matrix composites is a new technique, which is achieved by adding element and compound powder or performs into the molten aluminum. In the case of in situ synthesis, the desired reinforced particles can be synthesized directly using the chemical reaction between the reactants in the melt [4]. In situ reaction processes involving particle-reinforced composite systems eliminate interfacial compounds in favor of nucleation and growth from the parent matrix phase to form more thermodynamically stable reinforced compounds. Meanwhile, the composites possess contaminant-free reinforcement/matrix interfaces, and the in situ  $\text{Al}_2\text{O}_3$  particles are fine and can enhance the strength and ductility of the composite. Compared with the previous techniques, advantages are as follows: (i) the distribution of the in situ reinforcements are more homogeneous in the whole microstructures and more thermodynamically stable; (ii) the in situ reinforcements have a metallurgical bonding with the matrix, which results in a strong interfacial bonding between the reinforcements and the matrix. Recently, some metal oxides (e.g.,  $\text{Fe}_2\text{O}_3$ ,  $\text{MnO}_2$ , and  $\text{CuO}$ ) were added to molten aluminum to produce  $\text{Al}_2\text{O}_3$  particle reinforcement with a high performance, low cost, and good wettability, which can take the external load and the good interfacial cohesion between  $\text{Al}_2\text{O}_3$  and the matrix [4]. In an in situ Al/CuO composite system, oxygen atoms diffuse along the powder surfaces and the lattice and grain boundaries during synthesis, and an oxide film on the surface of a metal powder has a significant effect on the bonding properties of the powder. In this case, the oxide film can accelerate the bonding between particles when the film thickness is less than critical. The in situ SLM reaction of Al/ $\text{Fe}_2\text{O}_3$  powder mixtures released extra heat and collaborated with laser energy, which can modify the visual surface and microstructural appearance or alter material characteristics, and the hardness of composite was increased [5]. Further taking the  $\text{Al}_2\text{O}_3$  as the raw material, the high-performance  $\text{Al}_2\text{Si}_4\text{O}_{10}$  reinforced aluminum was in situ synthesized by powder metallurgy technique and the resultant mechanical properties of AMCs was considerably enhanced [6]. Although the presence of reinforcements in situ synthesized in the aluminum composites can strengthen the performance of the corresponding aluminum matrix efficiently, the conventional AMCs reinforced by in situ synthesized reinforcements using micro-scale particles commonly have a remarkably coarse microstructure with attendant poor mechanical performance resulting from a slow cooling rate in traditional manufacturing processes [7].

Additive manufacturing (AM)/3D printing (3DP) refers to the process of fabricating three-dimensional near-net-shaped components directly from powder particles in a layer-by-layer manner. It enables a number of technical and economic advantages, e.g., improving the cost-competitiveness for low volume production, reducing the environmental impact of manufacture, and increasing design complexity [8]. Selective laser melting (SLM), a newly developed AM/3DP process, is based on the principle of material incremental manufacturing and considered a promising AM technology for metallic parts, due to its flexibility in feedstock and shapes. SLM provides possibilities to fabricate the geometrically complex components by user-defined computer-aided design (CAD) files without tools or molds that would be difficult to develop by conventional manufacturing methods. It enables the quick fabrication of the geometry- complex components directly from powders. Under the irradiation of the high-energy laser beam, SLM fabricates parts in a layer-wise fashion by selectively fusing and consolidating the thin layers of the loose powder [9]. Generally, the geometrically complex components are fabricated by SLM with a high dimensional precision and good surface integrity without other subsequent process requirements, which the conventional

techniques (e.g., casting and machining) cannot keep pace with easily [10]. Moreover, during SLM, the temperature of the powder-bed where the applied high energy laser beam is irradiated reaches a maximum temperature of  $10^5$  K, and is followed by a rapid cooling at a rate up to  $10^{6-7}$  K/s as the laser beam moves away, which involves a rapidly melted and solidified powder metallurgical mechanism and affects the forging of non-equilibrium phases with fine grained microstructures with superior metallurgical properties [11,12]. In this case, due to the extremely large cooling rate, a considerably fine microstructure is obtained, and the resultant performances are efficiently enhanced. The application of SLM in the fabrication of AMCs is expected to create newly mechanical and technological opportunities, because of the potential for developing novel in situ composites with unique mechanical properties.

Previous research has mainly been focused on the fabrication of high-performance AMCs by SLM using ceramic particles, such as TiC [13], AlN [14], and B<sub>4</sub>C [15]. Although the above-mentioned AMCs fabricated by SLM enhance the mechanical properties, a poor bonding strength between the reinforcements and the aluminum was also generated. To date, there are very few studies on in situ oxide dispersion-strengthened (ODS) AMCs fabricated by SLM, which are believed to possess unmatched advantages compared with the conventional components. AlSi10Mg is normally used in the automotive industry for its high specific strength, in applications where fatigue performance is also critical. Therefore, according to the excellent properties of Al<sub>2</sub>Si<sub>4</sub>O<sub>10</sub>, this paper focuses on the in situ synthesized Al<sub>2</sub>Si<sub>4</sub>O<sub>10</sub> ODS Al-based composites and the attendant growth mechanism. The Al<sub>2</sub>O<sub>3</sub>/AlSi10Mg composite powders were prepared by the processing of high-energy ball milling; subsequently, the Al<sub>2</sub>Si<sub>4</sub>O<sub>10</sub>/Al composites were produced by SLM to obtaining desirable parts with novel microstructures. The attendant chemical composition, the microstructure characterization, and the formation mechanism of the composites were studied in detail.

## 2. Materials and Methods

### 2.1. Preparation of Samples

The gas atomized pre-alloy powders of AlSi10Mg powder (a purity of 99.7%) were used as the starting material with a near spherical shape and a mean particle size of 30  $\mu$ m. The Al<sub>2</sub>O<sub>3</sub> powders (a purity of 99.5%) with a polygonal morphology and a mean particle size of 9  $\mu$ m were used as reinforcements. The Al<sub>2</sub>O<sub>3</sub>/AlSi10Mg composite powders were mechanically milled with a weight ratio of 80:20 in a Fritsch Pulverisette 4 planetary mill (Idar-Oberstein, Germany), using a ball-to-powder weight ratio of 10:1, a rotation speed of 200 rpm, and a milling time of 8 h. As depicted in Figure 1a, the small-size reinforcements of Al<sub>2</sub>O<sub>3</sub> were homogeneously dispersed around the AlSi10Mg composite powders after milling. The SLM experimental system was developed by Nanjing University of Aeronautics and Astronautics and consisted of an YLR-500-SM Ytterbium fiber laser (Burbach, Germany) with a power of ~500 W and a spot size of 70  $\mu$ m, an automatic powder layering apparatus (Nanjing, China), an inert argon gas protection system, and a computer system for process control. The schematic of SLM processing is shown in Figure 1b. The detailed processing of the concerned SLM procedures is described in [16]. The samples were fabricated with dimensions of 8  $\times$  5  $\times$  5 mm<sup>3</sup>. Moreover, the corresponding processing parameters of SLM were set as follows: the power of the laser beam was settled at 100 W, 150 W, and 200 W, with a scan speed of 400 mm/s, a spot size of 70  $\mu$ m, a hatch spacing of 50  $\mu$ m, and a powder-bed thickness of 50  $\mu$ m.

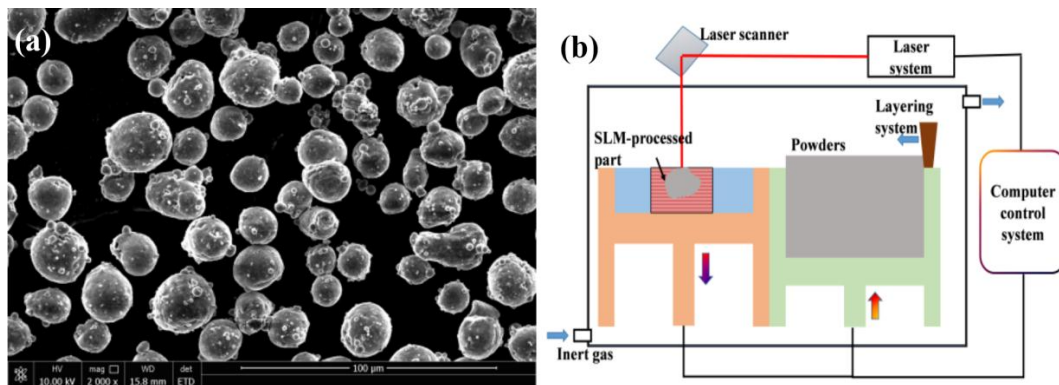


**Figure 1.** Morphologies of the homogeneously mixed  $\text{Al}_2\text{O}_3/\text{AlSi10Mg}$  composite powders processed by ball milling (a); the schematic of SLM processing (b).

## 2.2. Characterization of Composition

The SLM-processed specimens for metallographic examinations were cut, ground, and polished according to standard procedure, and then etched with a solution consisting of HF (1.0 mL), HCL (1.5 mL),  $\text{HNO}_3$  (2.5 mL), and distilled water (95 mL) for about 10 s. An Olympus PMG3 optical microscope (OM, Tokyo, Japan) was used to observe surface morphology of the SLM-processed specimens. X-ray diffraction (XRD, Karlsruhe, German) was employed to identify the phase. Microstructures were obtained with a field emission scanning electronic microscope (FE-SEM, Tokyo, Japan), which was equipped with EDX for the determination of chemical compositions.

## 2.3. Numerical Simulation

To further investigate the thermodynamic behavior within the molten pool during the selective laser melting  $\text{Al}_2\text{O}_3/\text{AlSi10Mg}$  composite, a physical model was established using a finite volume method (FVM) and the corresponding physical properties of materials was properly settled according to [17]. The heat and mass transfer, the surface tension induced by the temperature gradient, and the movement of laser beam power with a Gaussian energy distribution was taken into account in the numerical model. Moreover, the in situ reaction of  $\text{Al}_2\text{O}_3$  and  $\text{AlSi10Mg}$  was considered, and the resultant phase transition from  $\text{Al}_2\text{O}_3$  and  $\text{AlSi10Mg}$  to the in situ  $\text{Al}_2\text{Si}_4\text{O}_{10}$  reinforcements was taken into consideration, including the heat transition during SLM. Meanwhile, some assumptions were also addressed in our physical model:

- (1) The evaporation of molten liquid material was ignored when the maximum temperature of the molten material did not exceed the boiling temperature.
- (2) The reflectivity was regarded as a constant by varying the laser absorption of the aluminum alloy powder.
- (3) The conductivity and melt viscosity were considered to be time-dependent.

The effect of the applied laser power on the temperature distribution and velocity field was investigated. The temperature counter and velocity field of the Y-Z cross-section ( $X = 150 \mu\text{m}$ ) were obtained to investigate the influence of the laser power on the thermodynamic behavior within the molten pool during SLM.

## 3. Results and Discussion

### 3.1. Phases and Composition Identification

Figure 2 depicts the typical XRD spectrum of SLM-processed composites. It was evident that the peaks characterized with relatively strong diffraction intensities were identified as the aluminum

matrix, i.e., the AlSi10Mg phase. Meanwhile, the primary phase of Si was also generated during SLM, which was mainly consistent with the previous reports. The diffraction peaks with relatively weak intensity corresponding to the new silica-rich phase (aluminum silicate, i.e.,  $\text{Al}_2\text{Si}_4\text{O}_{10}$ ) was identified, revealing the general formation of the in situ synthesized  $\text{Al}_2\text{Si}_4\text{O}_{10}$  reinforced AMCs.

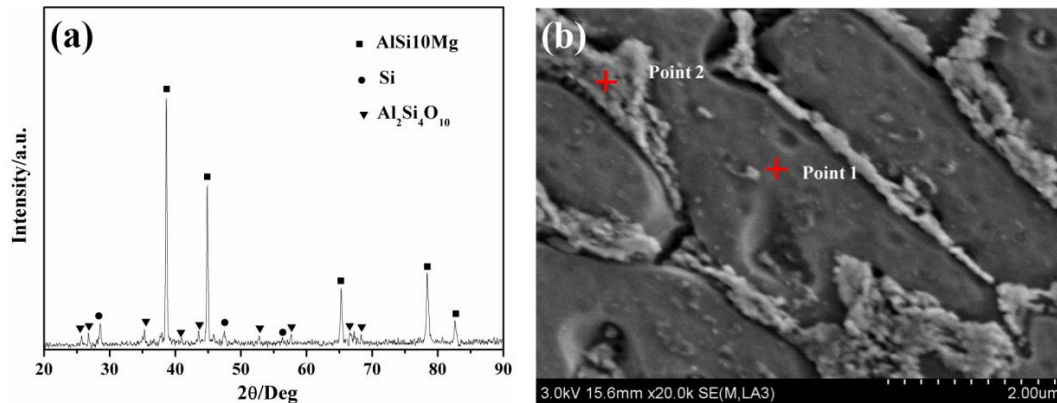


**Figure 2.** XRD spectrum (a) and the field emission scanning electronic microscope (FE-SEM) images showing the characteristic microstructure (b) of the SLM-processed composites at 150W and 400 mm/s.

The microstructure of SLM-processed composites is shown in Figure 2b. It was clearly observed that the quite fine cellular microstructure was obtained with an ellipse shape. EDX spectra of the two different phases above were obtained to determine their respective chemical composition quantitatively, and the relevant results are illustrated in Table 1. It was revealed that the phase (Point 1, Figure 2b) was rich in Al elements with a small amount of Si and O elements dissolved in the aluminum matrix, which was considered the aluminum matrix. The higher concentration of oxygen could have been ascribed to the diffusion of the  $\text{Al}_2\text{O}_3$  reinforcement. On the other hand, the molten liquid aluminum tended to oxidize during SLM due to the residual oxygen within the operating chamber [11], whereas the phase (Point 2, Figure 2b) was mainly composed of Al, Si, and O elements with an atomic ratio of approximate 2:4:10, which revealed that the new phase of in situ synthesized  $\text{Al}_2\text{Si}_4\text{O}_{10}$  reinforcements were generated. Moreover, as seen from the EDX results, the high cooling rate induced by SLM can effectively extend the solid solubility of Si in the aluminum matrix, leading to a supersaturated solid solution of 6.07%. Further analysis of the EDX result of the aluminum matrix indicated SLM could largely extend the solid solubility of Si in  $\alpha$ -Al, leading to a supersaturated solid solution of 6.07%. Thus, it is reasonable to conclude that the in situ  $\text{Al}_2\text{Si}_4\text{O}_{10}$  phase was generated, and the attendant in situ  $\text{Al}_2\text{Si}_4\text{O}_{10}$ / $\text{AlSi10Mg}$  composites were successfully prepared by SLM combined with the XRD and EDX results.

**Table 1.** EDX element analysis of Point 1 and Point 2 in Figure 2b showing the chemical compositions in the SLM-processed  $\text{Al}_2\text{Si}_4\text{O}_{10}$ / $\text{AlSi10Mg}$  composites.

Position	Elements (at. %)			
	Al	Si	O	Mg
Point 1	89.1	5.75	4.74	0.41
Point 2	12.56	24.98	62.46	-

### 3.2. Microstructure Characterization

The typical microstructures on the cross-section of SLM-processed composites at variable laser powers are shown in Figure 3. As a relatively low laser power of 100 W was used, the characteristic microstructure presented in a network structure and appeared to be irregular. Moreover, a considerable

number of irregular  $\text{Al}_2\text{Si}_4\text{O}_{10}$  reinforcements were evidently observed with a nearly nano-scale diameter. They were highly inclined to connect with each other coherently and aggregated into clusters in a fairly large region of the SLM-processed composites (marked by white dash lines in Figure 3a). SLM is widely known to be characterized by an extremely large cooling rate as high as  $10^{6-8}$  K/sin, a low laser energy density, and a small lifespan of the molten pool. In this situation, reinforcements would spread insufficiently and tended to aggregate in most of the regions of the composites [12]. As the laser power was increased to 150 W, the microstructure was observed with an ellipse shape, and the  $\text{Al}_2\text{Si}_4\text{O}_{10}$  reinforcements were distributed along the boundary of the Al matrix. However, a slight number of  $\text{Al}_2\text{Si}_4\text{O}_{10}$  reinforcements were aggregated in a certain region of the composites (marked by white dash lines in Figure 3b). As the laser power was elevated to 200 W, the in situ  $\text{Al}_2\text{Si}_4\text{O}_{10}$  reinforcements were exhibited along the boundary of Al matrix in a nearly sphere-like forming. Meanwhile, the network microstructure of SLM-processed composite performed regularly (Figure 3c). This phenomenon was attributed to Marangoni convection [2,17]. As a large laser power was used, a considerable intensity of Marangoni convection was obtained, which evidently favored the sufficient spreading of reinforcements. Thus, the reinforcements could be distributed uniformly under a reasonable laser power. The AlSi10Mg molten liquid was formed due to the actions of laser beam source irradiated the powder-bed system, and unimpeded motion of molten aluminum into the interconnected network of channels and crevices occurs between  $\text{Al}_2\text{O}_3$  particles via capillary action. Under this situation, the  $\text{Al}_2\text{Si}_4\text{O}_{10}$  reinforcements existing around the AlSi10Mg matrix obviously disappear.

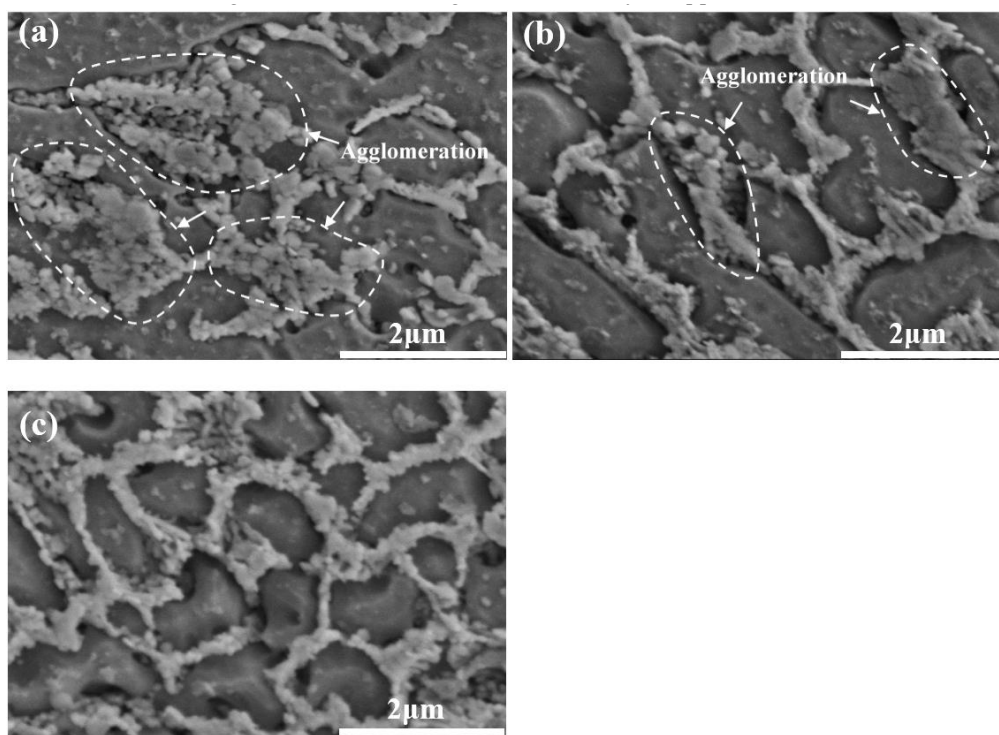


**Figure 3.** FE-SEM images of the microstructures of SLM-processed composites at 100 W, 400 mm/s (a); 150 W, 400 mm/s (b); 200 W, 400 mm/s (c).

### 3.3. Thermodynamic Behavior of Molten Pool

The calculated temperature counter and velocity fields within the molten pool in the cross-sectional view at variable laser power are shown in Figure 4. According to the temperature contour plots, it was clear that the peak temperature presented at the center underneath the laser beam with Gaussian distribution and decreased radially outward. The peak temperature was elevated

ranging from 1350 K to 1760 K by increasing the laser power. Meanwhile, the temperature gradients were observed to be varied with variable laser power, resulting in the formation of Marangoni convection within the molten material shown on the right side of each picture in Figure 4. It is evident that the velocity of the molten material is enhanced by increasing the laser power. This is attributed to the decrease in the dynamic viscosity ( $\mu$ ) of the molten material and the surface tension ( $\gamma$ ) [17–20]. The peak temperature of the simulation on SLM-processed composites was far below the melting point of reinforcements, leading to the reinforcements remaining solid in the molten pool. Thus, it was reasonable to consider that the reinforcements within the molten pool tended to migrate under Marangoni convection. Accordingly, the intensity of the velocity of the molten material significantly affects the dispersion states of the reinforcements. A low laser power also weakened the Marangoni convection and the attendant thermal capillary forces, thereby slowing down the molten liquid flow and migration of reinforcements. Consequently, the nano-scaled solid reinforcements tended to aggregate within the molten pool under the action of each particle, resulting in a severe agglomeration of the reinforcing particulates. By increasing the applied laser power to 150 W, the recirculation was intensified, and the distribution state of reinforcement can thus be enhanced. As a large laser power of 200 W was applied, a high peak temperature was obtained and resultant Marangoni convection was generated with a low viscosity and a high motioning velocity, favoring the sufficient dispersion of the reinforcements within the molten pool. On the other hand, repulsive forces prefer to strengthen between  $\text{Al}_2\text{Si}_4\text{O}_{10}$  reinforcements when the amount of Al melt is sufficient in the molten pool [21]. In the combined effect of Marangoni convection and repulsion forces, the dispersive network-structure of the  $\text{Al}_2\text{Si}_4\text{O}_{10}$ -reinforced Al matrix is accordingly obtained at the appropriate SLM conditions. Thus, a reasonable laser power is beneficial for obtaining a homogeneous distribution of reinforcement in the aluminum matrix.

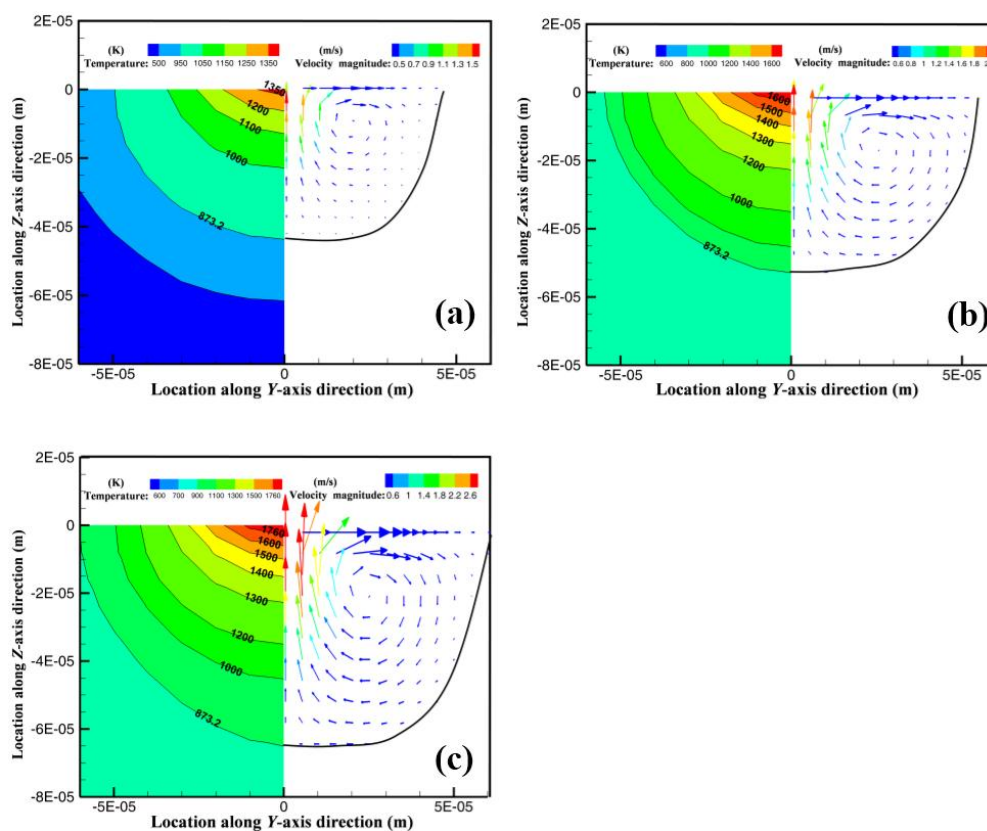
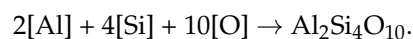


**Figure 4.** Simulated temperature counter and velocity fields within the melt pool in the cross-sectional view at different processing parameters: (a) 100 W, 400 mm/s; (b) 150 W, 400 mm/s; (c) 200W, 400 mm/s.

### 3.4. Formation Mechanism of SLM-Processed Composites

Zawrah et al. [6] designed and prepared  $\text{Al}_2\text{O}_3$ -SiC-mullite reinforced Al-based composites by reaction sintering; meanwhile, new silica phase  $\text{Al}_2\text{Si}_4\text{O}_{10}$  was found by decreasing the amount of mullite. Zawrah considered that the formation of the  $\text{Al}_2\text{Si}_4\text{O}_{10}$  phase might be attributed to the reaction between  $\text{Al}_2\text{O}_3$  and  $\text{SiO}_2$ . Similarly, for the SLM-processed Al-based composites in this study,  $\text{Al}_2\text{O}_3$  also acted as a raw material. To explicitly illustrate the formation mechanism of in situ  $\text{Al}_2\text{Si}_4\text{O}_{10}$  during SLM processing, the corresponding schematic diagram is shown in Figure 5a. As the laser beam fleetly moves over the powder bed, powder particles melt rapidly, and the temperature within the formed tiny molten pool shows a heterogeneous distribution due to the usage of a Gaussian heat source. Consequently, a surface tension gradient emerged due to the existence of a temperature gradient, resulting in the formation of Marangoni convection. Based on an investigation by Gu et al. [22],  $\text{Al}_2\text{O}_3$  particles are continuously pushed and gather under the combined effects of Marangoni convection and torque around the particle, forming a ring-like structure observed in Figure 3. According to the Gibbs–Kelvin formula, fine embossment existing on the surface of an  $\text{Al}_2\text{O}_3$  particle can give rise to a remarkable increase in saturated vapor pressure, thus contributing to the partial melting behavior of the  $\text{Al}_2\text{O}_3$  particle. As a result, part of the dissociative [Al] and [O] atoms were released into the molten pool and interacted with dissociative [Si] atoms in the melt. The reaction could be described as



During the in situ reaction, the  $\text{Al}_2\text{O}_3$  particle acted as the oxygen resource, providing sufficient [O] atoms for the formation of the new phase  $\text{Al}_2\text{Si}_4\text{O}_{10}$ . Hence, the aluminum silicate phase precipitated attachment to the remaining  $\text{Al}_2\text{O}_3$  particles.

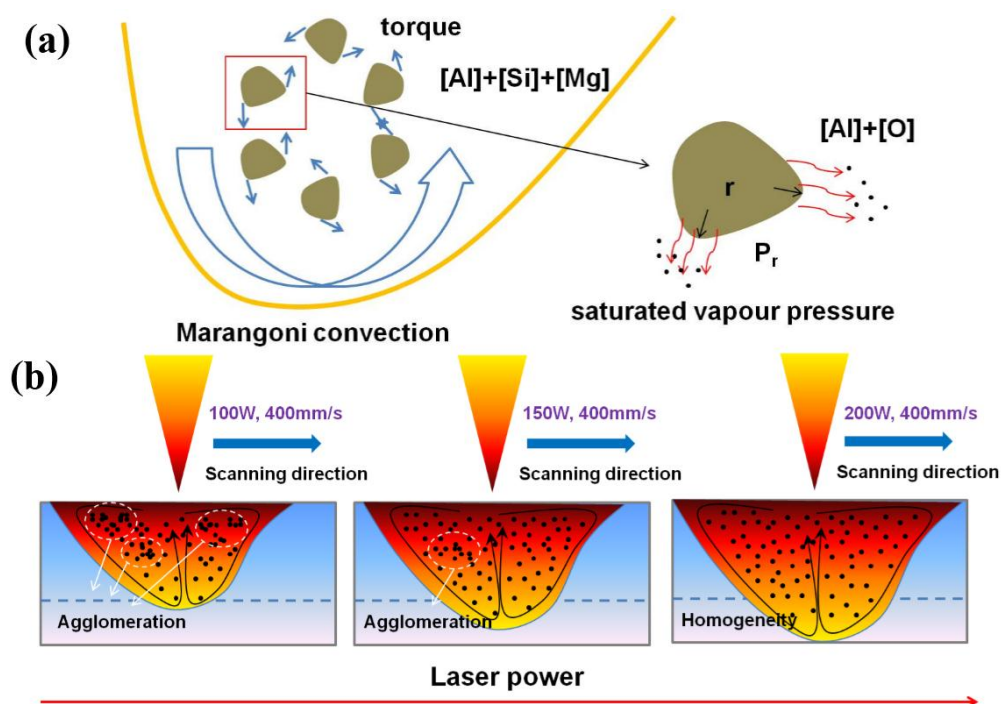


**Figure 5.** Schematic of the formation mechanism of the in situ  $\text{Al}_2\text{Si}_4\text{O}_{10}$  phase (a) and particle distribution (b) during SLM processing.

Based on the above experiment results, it has been concluded that laser energy input can significantly influence the distribution of ex-situ  $\text{Al}_2\text{O}_3$  and in situ  $\text{Al}_2\text{Si}_4\text{O}_{10}$  particles within the molten pool. The underlying factor contributing to the dispersion state of reinforcement is the input energy

and resultant operative temperature [23–25]. For a clearer understanding of the distribution evolution of reinforcement particles, the corresponding schematics are shown in Figure 5b. At a relatively low laser power, the temperature within the molten pool is limited, consequently increasing the viscosity of the melt and weakening Marangoni convection. Moreover, the nucleation sites of the  $\text{Al}_2\text{Si}_4\text{O}_{10}$  phase are confined to the top region of the molten pool. Under the weak Marangoni convection,  $\text{Al}_2\text{O}_3$ – $\text{Al}_2\text{Si}_4\text{O}_{10}$  multi-particles drive toughly toward the boundary of the molten pool and finally agglomerate in the solidified front. As the applied laser power increases, the Marangoni convection is remarkably enhanced due to the elevated temperature within the molten pool, thus accelerating the migration of reinforcement particles toward the bottom part of the molten pool. Taking into account the limited temperature rise, agglomeration still occurs when reinforcement particles are migrated to the middle region of the molten pool. As laser power further increases, the nucleation sites of the  $\text{Al}_2\text{Si}_4\text{O}_{10}$  phase significantly increase; meanwhile, the Marangoni convection is strong enough to guarantee the homogenous distribution of reinforcement particles.

#### 4. Conclusions

- (1) The in situ  $\text{Al}_2\text{Si}_4\text{O}_{10}$ /Al composites were fabricated via SLM. The new silica-rich phase (aluminum silicate, i.e.,  $\text{Al}_2\text{Si}_4\text{O}_{10}$ ) was identified via XRD spectrum and EDX analysis. The composites also presented a network microstructure, i.e., the  $\text{Al}_2\text{Si}_4\text{O}_{10}$  reinforcements aggregated around the aluminum matrix.
- (2) The characteristic microstructure of the in situ  $\text{Al}_2\text{Si}_4\text{O}_{10}$ /Al composites via SLM tended to transfer from the irregular network structure to a nearly sphere-like network structure in regular forming by increasing the laser power.
- (3) As a high laser power was employed, a high peak temperature was acquired correspondingly, and the resultant Marangoni convection was generated with a high velocity, favoring the sufficient dispersion of the reinforcements within the molten pool.
- (4) The formation mechanism of in situ  $\text{Al}_2\text{Si}_4\text{O}_{10}$  and the distribution evolution of the reinforcement particles during the SLM processing of  $\text{Al}_2\text{O}_3$ /AlSi10Mg mixed powder were present. Formation of the in situ  $\text{Al}_2\text{Si}_4\text{O}_{10}$  phase could be attributed to the reaction among dissociative [Al], [O], and [Si] atoms, and the distribution of reinforcement particles was speculated to be influenced significantly by Marangoni convection and the viscosity of the molten material.

**Acknowledgments:** The authors gratefully acknowledge the financial support from the Shanghai Aerospace Science and Technology Innovation Fund (No. SAST2015053).

**Author Contributions:** D.D. Gu, J.B. Jue, and M.J. Xia formulated this research with cooperation from L.F. Wang and L.J. Guo. J.B. Jue and M.J. Xia performed the experimental and simulation work, with the help of D.D. Gu, interpreted the results, and prepared and revised the manuscript. All co-authors contributed to manuscript proof and submissions.

**Conflicts of Interest:** The authors declare no conflict of interest.

#### References

1. Tjong, S.C. Novel Nanoparticle-Reinforced Metal Matrix Composites with Enhanced Mechanical Properties. *Adv. Eng. Mater.* **2007**, *9*, 639–652. [[CrossRef](#)]
2. Gu, D.D.; Yuan, P.P. Thermal evolution behavior and fluid dynamics during laser additive manufacturing of Al-based nanocomposites: Underlying role of reinforcement weight fraction. *J. Appl. Phys.* **2015**, *118*, 233109. [[CrossRef](#)]
3. Vijaya Ramnath, B.; Elanchezian, C.; Jaivignesh, M.; Rajesh, S.; Parswajinan, C.; Siddique Ahmed Ghias, A. Evaluation of mechanical properties of aluminium alloy-alumina-boron carbide metal matrix composites. *Mater. Des.* **2014**, *58*, 332–338. [[CrossRef](#)]
4. Yang, B.; Sun, M.; Gan, G.S.; Xu, C.G.; Huang, Z.J.; Zhang, H.B.; Fang, Z.Z. In situ  $\text{Al}_2\text{O}_3$  particle-reinforced Al and Cu matrix composites synthesized by displacement reactions. *J. Alloy. Compd.* **2010**, *494*, 261–265. [[CrossRef](#)]

5. Dadbakhsh, S.; Hao, L.; Jerrard, P.G.E.; Zhang, D.Z. Experimental investigation on selective laser melting behaviour and processing windows of in situ reacted Al/Fe<sub>2</sub>O<sub>3</sub> powder mixture. *Powder Technol.* **2012**, *231*, 112–121. [[CrossRef](#)]
6. Zawrah, M.F.; Aly, M.H. In situ formation of Al<sub>2</sub>O<sub>3</sub>-SiC-mullite from Al-matrix composites. *Ceram. Int.* **2006**, *32*, 21–28. [[CrossRef](#)]
7. Olakanmi, E.O.; Cochrane, R.F.; Dalgarno, K.W. A review on selective laser sintering/melting (SLS/SLM) of aluminium alloy powders: Processing, microstructure, and properties. *Prog. Mater. Sci.* **2015**, *74*, 401–477. [[CrossRef](#)]
8. Leary, M.; Mazur, M.; Elambasseril, J. Selective laser melting (SLM) of AlSi12Mg lattice structures. *Mater. Des.* **2016**, *98*, 344–357. [[CrossRef](#)]
9. Prashanth, K.G.; Scudino, S.; Chaubey, A.K.; Löber, L.; Wang, P.; Attar, H.; Schimansky, F.P.; Pyczak, F.; Eckert, J. Processing of Al-12Si-TNM composites by selective laser melting and evaluation of compressive and wear properties. *J. Mater. Res.* **2016**, *31*, 55–65. [[CrossRef](#)]
10. Attar, H.; Löber, L.; Funk, A.; Calin, M.; Zhang, L.C.; Prashanth, K.G.; Scudino, S.; Zhang, Y.S.; Eckert, J. Mechanical behavior of porous commercially pure Ti and Ti-TiB composite materials manufactured by selective laser melting. *Mater. Sci. Eng. A* **2015**, *625*, 350–356. [[CrossRef](#)]
11. Gu, D.D.; Meiners, W.; Wissenbach, K.; Poprawe, R. Laser additive manufacturing of metallic components: Materials, processes and mechanisms. *Int. Mater. Rev.* **2012**, *57*, 133–164. [[CrossRef](#)]
12. Das, M.; Balla, V.K.; Basu, D.; Bose, S.; Bandyopadhyay, A. Laser processing of SiC-particle-reinforced coating on titanium. *Scr. Mater.* **2010**, *63*, 438–441. [[CrossRef](#)]
13. Gu, D.D. *Laser Additive Manufacturing of High-Performance Materials*; Springer: Berlin/Heidelberg, Germany, 2015; pp. 175–197.
14. Dai, D.H.; Gu, D.D. Influence of thermodynamics within molten pool on migration and distribution state of reinforcement during selective laser melting of AlN/AlSi10Mg composites. *Int. J. Mach. Tool. Manu.* **2016**, *100*, 14–24. [[CrossRef](#)]
15. Chang, F.; Gu, D.D.; Dai, D.H.; Yuan, P.P. Selective laser melting of in situ Al<sub>4</sub>SiC<sub>4</sub> + SiC hybrid reinforced Al matrix composites: Influence of starting SiC particle size. *Surf. Coat. Tech.* **2015**, *272*, 15–24. [[CrossRef](#)]
16. Gu, D.D.; Shen, Y.F. WC-Co particulate reinforcing Cu matrix composites produced by direct laser sintering. *Mater. Lett.* **2006**, *60*, 3664–3668. [[CrossRef](#)]
17. Yuan, P.P.; Gu, D.D.; Dai, D.H. Particulate migration behavior and its mechanism during selective laser melting of TiC reinforced Al matrix nanocomposites. *Mater. Design.* **2015**, *82*, 46–55. [[CrossRef](#)]
18. Read, N.; Wang, W.; Essa, K.; Moataz, M.A. Selective laser melting of AlSi10Mg alloy: Process optimization and mechanical properties development. *Mater. Design.* **2015**, *65*, 417–424. [[CrossRef](#)]
19. Zhang, B.C.; Bi, G.J.; Nai, S.; Sun, C.N.; Wei, J. Microhardness and microstructure evolution of TiB<sub>2</sub> reinforced Inconel 625/TiB<sub>2</sub> composite produced by selective laser melting. *Opt. Laser Technol.* **2016**, *80*, 186–195. [[CrossRef](#)]
20. Wang, D.; Song, C.H.; Yang, Y.Q.; Bai, Y.C. Investigation of crystal growth mechanism during selective laser melting and mechanical property characterization of 316L stainless steel parts. *Mater. Design.* **2016**, *100*, 291–299. [[CrossRef](#)]
21. Gu, D.D.; Shen, Y.F.; Wu, X.J. Formation of a novel W-rim/Cu-core structure during direct laser sintering of W-Cu composite system. *Mater. Lett.* **2008**, *62*, 1765–1768. [[CrossRef](#)]
22. Gu, D.D.; Wang, H.Q.; Dai, D.H. Rapid fabrication of Al-based bulk-form nanocomposites with novel reinforcement and enhanced performance by selective laser melting. *Scr. Mater.* **2015**, *96*, 25–28. [[CrossRef](#)]
23. Kurt, H.I.; Oduncuoglu, M. Formulation of the Effect of Different Alloying Elements on the Tensile Strength of the in situ Al-Mg<sub>2</sub>Si Composites. *Metals* **2015**, *5*, 371–382. [[CrossRef](#)]
24. Casati, R.; Vedani, M. Metal Matrix Composites Reinforced by Nano-Particles. *Metals* **2014**, *4*, 65–83. [[CrossRef](#)]
25. Subramanian, J.; Seetharaman, S.; Gupta, M. Processing and Properties of Aluminum and Magnesium Based Composites Containing Amorphous Reinforcement: A Review. *Metals* **2015**, *5*, 743–762. [[CrossRef](#)]

